ELSEVIER

Earth and Planetary Science Letters 200 (2002) 147–157

EPSL

www.elsevier.com/locate/epsl

Diffusive properties of fluid-filled grain boundaries measured electrically during active pressure solution

Siese de Meer [a,*], Christopher J. Spiers [a], Colin J. Peach [a], Tohru Watanabe [b]

[a] *High Pressure and Temperature Laboratory, Faculty of Earth Sciences, Utrecht University, PO Box 80.021, 3508 TA Utrecht, Netherlands*

[b] *Department of Earth Sciences, Toyama University, Gofuku 3190, Toyama 930-8555, Japan*

Received 1 October 2001; received in revised form 7 March 2002; accepted 7 March 2002

Abstract

Diffusion through 'wetted' grain boundaries is often the rate limiting process during rock deformation by intergranular pressure solution. However, the underlying processes operative within such boundaries are poorly understood. In this contribution we have studied the diffusive properties of wetted grain boundaries by measuring the electrical resistivity of single, annular halite–glass contacts undergoing active pressure solution. Optical observation shows continuous growth (i.e. widening) of the annular contacts by pressure solution. From the resistivity measurements and making use of the Nernst–Einstein equation, it was possible to calculate the apparent grain boundary diffusion coefficient $Z = D\delta C$ (i.e. the product of grain boundary diffusion coefficient D, grain boundary film thickness δ and the solubility C of the diffusing species in the grain boundary fluid) during the pressure solution process. The Z-values obtained lie in the range 3×10^{-20}–2×10^{-18} m^3/s, show an inverse dependence on normal stress (σ_n) and agree well with values inferred previously from single contact and polycrystalline compaction experiments.

Keywords: pressure solution; resistivity; grain boundaries; diffusion; halite

1. Introduction

Weakening of rock by water has been demonstrated in numerous field and laboratory studies. One of the principle effects is the role of water present in grain boundaries. Grain boundary water supports a fast intergranular diffusion path, which allows stress-driven mass transport, resulting in permanent, time-dependent deformation [1–11]. This process of dissolution–precipitation creep or pressure solution is an important mechanism of compaction in sedimentary rocks [12], of healing, sealing and strength recovery in active fault zones [13–18], of deformation under low temperature metamorphic conditions [4,19,20], and of evaporite flow [10,21,22]. It involves dissolution of material at grain contacts under high normal stress, diffusion through the grain boundary fluid phase, and precipitation at grain contacts under low normal stress or on free pore walls [4,7,21,23,24].

* Corresponding author. Tel.: +31-30-253-1177; Fax: +31-30-253-7725.

E-mail address: s.demeer@geo.uu.nl (S. de Meer).

0012-821X/02/$ – see front matter
PII: S0012-821X(02)00585-X

Since interfacial reactions and diffusion occur serially during pressure solution creep, either the grain boundary diffusive properties or interface reaction kinetics control the rate of the process. However, the elementary diffusive and interfacial processes operative within wetted grain boundaries are poorly understood, preventing adequate quantification of pressure solution rates in rock materials. In particular, the structure and diffusive properties of water-bearing grain boundaries have been a subject of debate for decades. It has been argued that water may be present in the form of (i) strongly adsorbed thin films [3,4,25–29], (ii) isolated inclusion or connected crack arrays [30,31], (iii) non-equilibrium or dynamically wetting channel networks or films ([7,19,23,32,33]; cf. [34]), or as (iv) a hydrated gel layer (Guéguen, pers. commun.).

Most experimental studies of pressure solution creep in crustal rocks have focussed on compaction of granular quartz [35–38]. However, the process is too slow in this and other rock-forming minerals to adequately determine even the bulk kinetics or the rate controlling mechanism, and the issues of grain boundary structure and properties remain a matter of speculation. A method of studying pressure solution within more practical time scales is to make use of highly soluble salts as model or 'rock analogue' materials. NaCl is a suitable material in which pressure solution phenomena are known to be rapid under ambient conditions [9,21] and the behaviour of which is directly relevant to salt tectonics [22]. Its pressure solution behaviour is relatively well understood on the basis of compaction, deformation and single grain contact experiments and appears to be diffusion controlled [9,21,26,27,33]. However, the internal structure, properties and wettability of the grain boundaries during pressure solution in NaCl remain controversial, principally because grain boundaries can be observed only after deformation ('post mortem' examination). Clearly then, progress in understanding and quantifying pressure solution creep in wet crustal rocks means that new techniques are needed to obtain basic data on the structure and properties of wet grain boundaries.

In an attempt to gain deeper insight into grain boundary properties and processes during pressure solution, we have performed electrical resistivity measurements on individual halite–glass contacts undergoing active, diffusion controlled pressure solution. Making use of the Nernst–Einstein relation, the resistivity data obtained are used to calculate the effective grain boundary diffusivity, $Z = D\delta C$ (m^3/s), where D is the solute diffusion coefficient in the grain boundary fluid (m^2/s), δ is the average grain boundary fluid thickness (m) and C (m^3/m^3) the solubility of the diffusing species.

2. Theoretical considerations

2.1. Principle of the present experiments

In the present experiments, the diffusive properties of a single, annular, NaCl–glass contact undergoing active pressure solution of the NaCl, in a sealed, miniature loading cell, are studied by measuring the electrical resistivity of the wetted contact (Fig. 1). Within the cell, a cleaved NaCl disc with a central conical hole is pressed coaxially onto a conical lens in the presence of saturated NaCl brine, so that a circular pressure solution contact is formed (Fig. 1). This circular contact, with mean radius r and width w, forms the only conduction path between a pair of circular platinum electrodes positioned in the free brine on opposite sides of the contact. Using the Nernst–Einstein equation, we relate the radial contact resistance to the quantity $Z = D\delta C$ within the dissolving contact.

2.2. Nernst–Einstein equation applied to the present configuration

The Nernst–Einstein equation relates the limiting molar conductivity ($\Lambda°_m$ in Sm^2/mol) of an electrolyte solution to the diffusion coefficient of the dissolved charge carrying ions and is written:

$$\Lambda^\circ_m = \frac{F^2}{RT}(\nu_+ Z_+^2 D_+ + \nu_- z_-^2 D_-) \quad (1)$$

where F is Faraday's constant, R is the gas con-

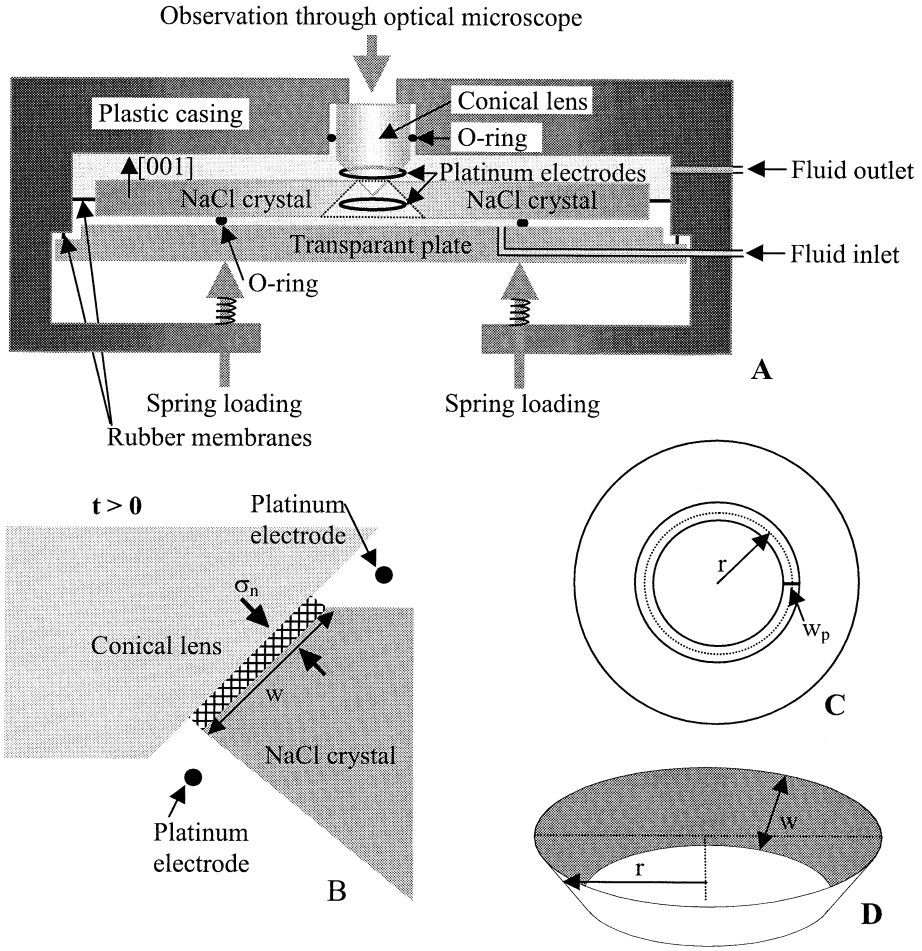

Fig. 1. Schematic diagram of the experimental configuration. (A) Experimental cell: axial section through the flat cylindrical body. At $t=0$, the NaCl disc (diameter 25 mm) just touches the conical lens forming an annular contact. (B) Close-up section of NaCl–lens contact after the start of the experiment ($t>0$): an NaCl–glass contact is formed by pressure solution under normal stress σ_n with progressively increasing width w and average fluid thickness δ. Note that the only path for conduction between the two platinum electrodes is through the NaCl–glass contact, i.e. through the diffusion path for pressure solution. (C) Vertical view of contact through lens at $t>0$, where w_p is the horizontal projection of contact width w. (D) Three-dimensional form of the dissolving contact at any time $t>0$, where r is the radius from the lens axis to the contact at $w/2$.

stant, T is the absolute temperature, ν_+ and ν_- are the numbers of cations and anions per formula unit of electrolyte, z_+ and z_- are the charge numbers of the cations and anions, and D_+ and D_- are their diffusion coefficients. In the case of a concentrated NaCl solution, since we are dealing with a strong electrolyte which is almost completely dissociated, we can write $\Lambda^\circ_m \approx \Lambda_m = \kappa / C_m$ where κ is the conductivity of the solution (Sm^{-1}), C_m is the concentration of NaCl in solution (mol/m^3) and where D_+ and D_- now take the significance of the effective diffusion coefficients of the sodium and chlorine ions with their associated hydration spheres [39]. Further we have $\nu_+ = \nu_- = 1$, $z_+ = z_- = 1$ and $D_+ = D_-$ for sodium and chlorine ions. Moreover, if the solution is saturated then $C_m = (C/V_m)$, where V_m is the molar volume of NaCl (m^3/mol) and C is the solu-

bility of NaCl in m^3/m^3. Hence the conductivity of a near saturated brine phase in a grain contact undergoing pressure solution can be written $\kappa = 2F^2DC_m/RT$. For our experimental configuration, the resistance (Ω) of the narrow annular contact (Fig. 1) to radial current flow by ionic conduction through the grain boundary fluid phase is given:

$$\Omega = \frac{w}{2\pi r \delta \kappa} \quad (2)$$

where δ is the average thickness of fluid in the grain contact, assuming negligible tortuosity in the internal conduction path, and w and r are the width and radius of the circular contact respectively (Fig. 1). Combining this with Eq. 1 yields for $Z = D\delta C$ (the product of the grain boundary diffusion coefficient, grain boundary thickness and concentration of ions in the grain boundary fluid) the expression:

$$Z = D\delta C = \frac{V_m RT}{4\pi F^2} \cdot \frac{w}{r} \cdot \frac{1}{\Omega} \quad (3)$$

where $V_m RT/4\pi F^2$ is a constant at constant temperature. Since the resistance of the open solution between electrodes and contact is negligible compared with the contact resistance, we can easily measure Ω and hence Z. Note here that even at constant temperature $Z = D\delta C$ is not necessarily a constant. Several authors have pointed out that mean intergranular fluid thickness δ may be stress dependent [3,4,27,28] and that both D and C may be (causally) related to δ (and perhaps even σ_n) when the grain boundary fluid is thin enough for surface forces to play a role [3,4].

3. Experimental method

As already indicated, our experimental cell (Fig. 1A) consists of two mutually isolated fluid reservoirs, one above and one below the disc-shaped NaCl crystal, with a circular platinum electrode located close to the crystal–lens contact in each reservoir. The annular NaCl–lens contact thus forms the only conduction path between the two electrodes. Force is applied to the contact by means of three adjustable springs, calibrated by replacing the lens with a push-rod linked to an electronic balance. The spring constants were chosen such that the applied load would remain constant within 2–4% during the duration of individual experiments, i.e. for the expected displacement of 100–200 μm due to pressure solution of the contact. Temperature is measured using a type K thermocouple positioned close to the NaCl–glass contact (not shown in Fig. 1A). The NaCl crystals used in our experiments were cleaved from cylindrical mother crystals, mechanically cored and ground to produce the conical central hole (1–2 mm diameter at the contact) and finally annealed at 700°C for 20 h to remove dislocation damage. The platinum electrodes were coated with platinum black to minimize polarization effects. Resistivity of the conduction path between the electrodes was measured using the setup illustrated in Fig. 2.

In setting up individual experiments, the apparatus is first assembled with the crystal sufficiently retracted to avoid contact with the lens. The springs are then engaged and the contact between crystal and lens is pre-loaded (dry) at the desired load for wet testing (1–5 N). It is subsequently unloaded so that the contact is fully re-opened. The cell is then filled completely with saturated brine via the lower reservoir, and the fluid in- and outlets closed. Spring loading is then reapplied with the result that the brine within the cell becomes pressurized. The conical lens and the rim of the central hole in the crystal are then brought into contact at the required load by bleeding out the excess brine from the cell, under the action of the springs. At this point, and then repeatedly after an interval of 1000 s, a programmable digital signal generator is activated, sending one 1 kHz sine wave burst to the platinum electrodes that has 3 s duration and 100 mV root mean square (RMS) amplitude. The alternating current (AC) flows via a 'current sense resistor', R_I, of 100 kΩ. The AC voltage drops, across this resistor, V_I, and cell, V_C, are amplified and measured, via RMS to direct current (DC) converters, to give simultaneously logged values of voltage and current from which the resistance of the cell, R_C, may be calculated using Ohm's law, ($R_C = V_C \times R_I / V_I$). An oscilloscope, in X/Y mode, is attached

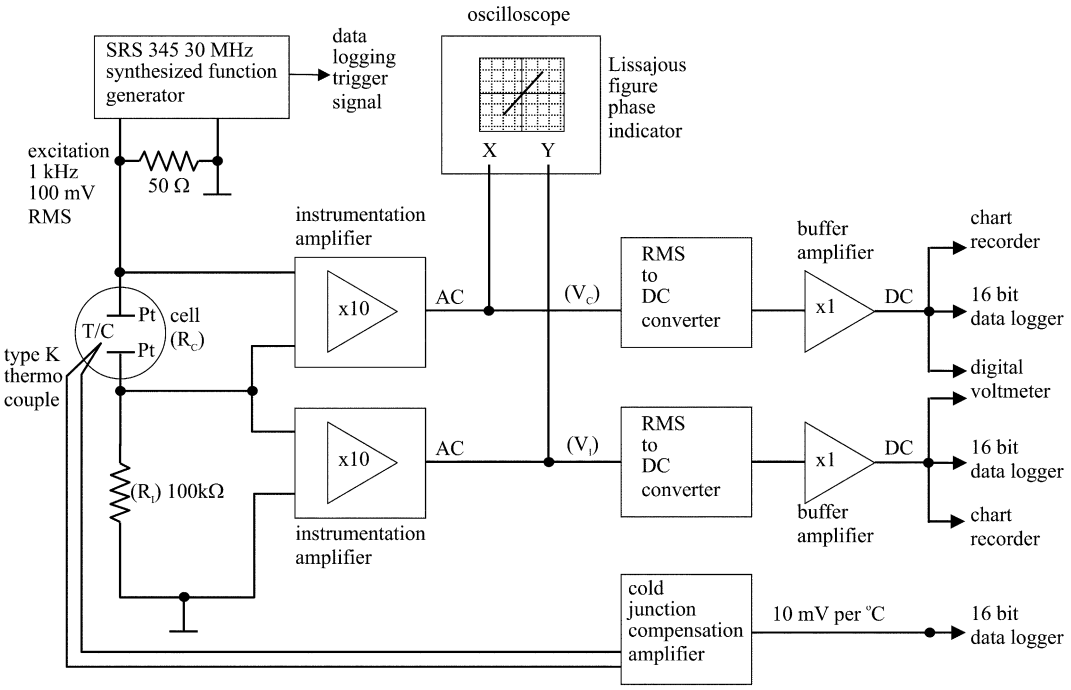

Fig. 2. Schematic diagram of experimental setup used to measure the resistivity of the conduction path between the two platinum electrodes.

to the AC signals, V_C to X and V_I to Y, to provide a visual indication of any electrical reactance. Any phase shift due to electrode capacitance or polarization will show as a departure from a line at 45° to the X-axis giving an elliptical Lissajous figure. Phase shifts were never greater than 5° using 1 kHz and 'platinum-blacked' electrodes. The frequency of 1 kHz was chosen after first checking the cell's frequency response with a Solartron 1260A impedance analyser. This showed purely resistive behaviour at 1 kHz. All voltages, including that from a conditioned type K thermocouple representing the cell temperature, were logged every 1000 s, to 16 bit precision by a multiplexed analogue to digital converter and microcomputer. The low excitation voltage of 100 mV and 3 s burst measurement every 1000 s were chosen to avoid minor contact heating effects inferred to occur at excitations ≥ 0.5 V. Widening of the loaded contact due to pressure solution is followed using an optical microscope and digital camera, enabling us to measure contact width (w) and radius (r) incrementally as a function of time, correcting for refractive index effects. The tests lasted typically up to 12 days, and were performed in a controlled climate room at a constant temperature of ~ 28°C. Normal stresses acting on the contact ranged from 1.5 to 20 MPa, though higher values must have been reached during initial contact formation when the contact width was too narrow to be reliably resolved. We report four experiments here, performed at applied forces of 1, 3 and 5 N. Note that no attempt was made to calculate pressure solution rates in these experiments, since the displacement of the crystal relative to the lens could not be sufficiently accurately measured in the cell used. Also, we made no attempt to investigate the surface structure of the dissolved contact after the experiments since the integrity of the surface could not be guaranteed when extracting the crystal from the cell (corruption by evaporation).

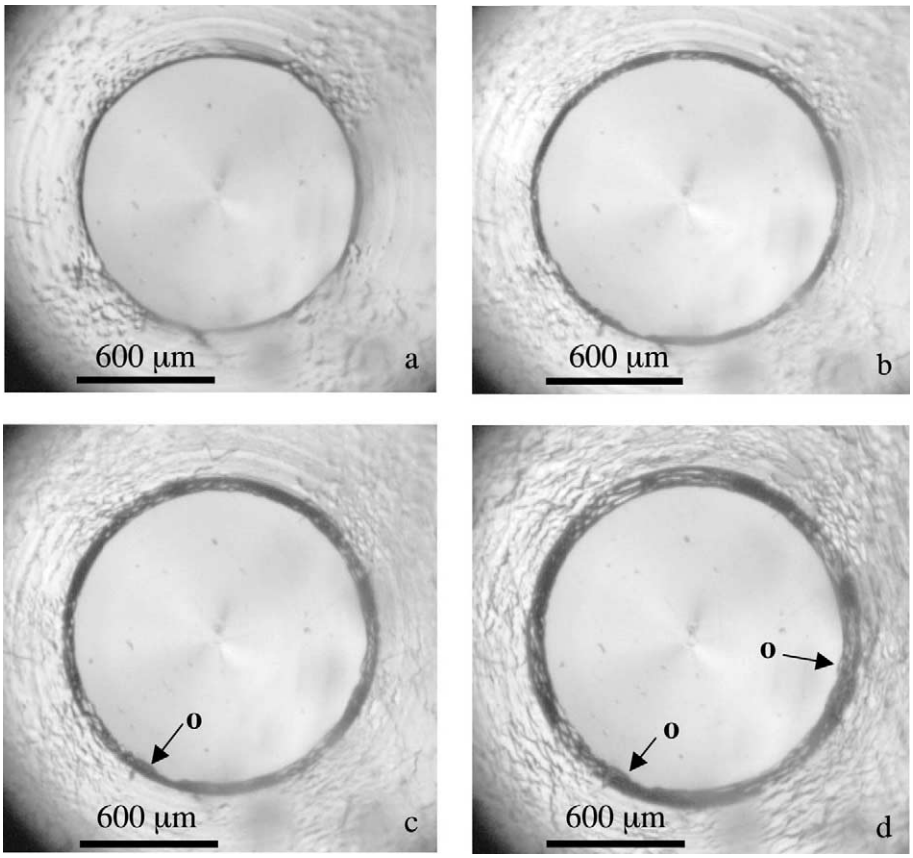

Fig. 3. Photographs illustrating contact development with time of experiment performed with applied force of 1 N at a temperature of 28°C. (a) Start of the experiment after the brine has been added and the conical lens is brought into contact with the NaCl again; (b) contact after ~1.8 days; (c) after ~4 days; and (d) after ~8 days. 'o' in c and d indicate overgrowths.

4. Results

4.1. Optical observations

At the start of each experiment, a narrow dark ring, of irregular width, appears immediately after the lens is brought into contact with the NaCl crystal. This disappears typically after about 2 h, then reappears after a further 20–24 h, growing continuously during the remainder of the experiment with remarkably uniform width. Fig. 3 illustrates this development in our 1 N experiment. Normal stresses at the contact range from ~5 MPa immediately after the start of this experiment to 1.8 MPa towards the end. Fig. 3a clearly shows the narrow, dark contact ring, observed at the start of the experiments, while in Fig. 3b–d the broadening of the re-formed contact with time is clearly visible. Idiomorphic overgrowths can be observed on the free surfaces near the crystal–lens contact ('o' in Fig. 3c,d) and on the (001) top surface of the crystal. Note that the concentric optical modulations, seen within (and outside) the dark contact ring (Fig. 3) are roughness developed on the machined conical surface of the NaCl crystal below the focal plane (refer Fig. 1) and not within the contact itself. This is verified by the fact that these features become increasingly out of focus, moving away from the contact. No optical structure could be observed within the circular contact.

4.2. Resistance data

Fig. 4a shows the contact resistance versus time curves obtained for all experiments reported. Note the marked differences between the curves.

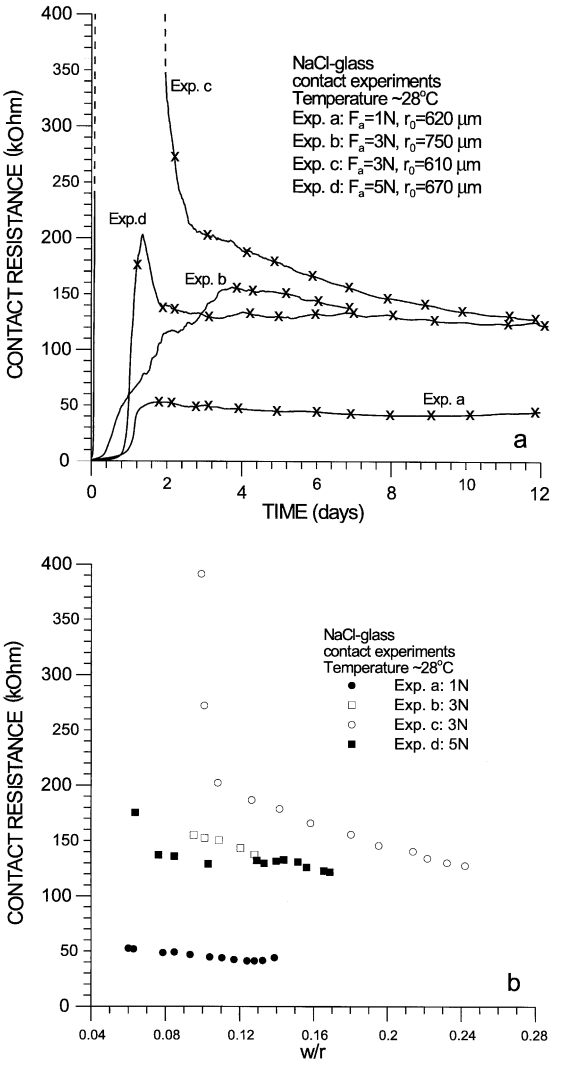

Fig. 4. (a) The contact resistance versus time curves for the present experiments. Applied forces (F_a) and initial radius of the contact (r_0) as indicated. Crosses (×) on the curves indicate points in time where optical photographs have been taken to measure contact width w and radius r. Note that Expt. c has a maximum around 1200 kΩ. (b) Contact resistance versus w/r. Note that the pre-peak data are not included because w could not be measured reliably.

The contact resistance increases from zero at varying rates in the beginning, reaching either a very sharp resistance peak after 1–1.5 days (Expts. c and d) or a broader maximum after 2–4 days (Expts. a and b). The resistance then falls towards a plateau value held for the remaining duration of the experiments.

The resistance data are plotted against normalized contact width (w/r) in Fig. 4b; the pre-peak data are not included as w could not be measured reliably. Note that the linear relation predicted by Eq. 2 is not obtained. Rather, the resistance is almost independent of w/r in the post-peak stage. Using Eq. 3 and the contact radius and width data obtained from the optical micrographs as a function of time, the resistance data have been reworked to compute (apparent) Z-values versus contact width w (Fig. 5a) and normal stress σ_n acting across the contact (Fig. 5b). Here too, values of Z are determined for points measured after the peak in the resistance vs. time plot (Fig. 4a), since these data fell within the phase of continuous growth of the re-formed contact and because the width was too small to be accurately measured in the first 1–2 days of the experiments. Fig. 5a shows that with increasing contact width Z also increases, suggesting a correlation between $Z = D\delta C$ and σ_n. This is illustrated in Fig. 5b which suggests that for normal stresses in the range 2 to 10 or 20 MPa, Z is inversely proportional to σ_n, though Expt. c shows a sharp drop in Z-values at stresses approaching the peak in resistance of 1200 kΩ (refer Fig. 4a).

5. Discussion

5.1. Resistance data and optical observations

Focussing on the resistance data, we have seen that during the first 1–2 days of the tests the contact resistance increases at widely varying rates from an initial value close to zero (Fig. 4a). In addition, during the first day, the initially present narrow dark ring disappears and then reappears as a continuously growing contact (Fig. 3), which we infer is undergoing pressure solution as expected. Our interpretation is that the initial dark

ring is simply an image of the rim of the hole in the upper surface of the crystal, with so few true contact points between rim and lens that the circular contact zone offers no resistance. Any plastic deformation of the contact points, which must occur under the action of the high contact stresses at the start of the tests [9], would already have occurred at this stage of the experiments. We propose that disappearance of the initial dark ring results from dissolution of the contact points and marks the formation of a more or less continuous contact, which is too narrow to be optically visible, but nonetheless causes substantial increase in resistance. We suggest that the increase in resistance varies from experiment to experiment, because of differing evolution of the completeness and degree of wetting of the contact. As the contact grows and becomes optically visible, resistance increases towards a sharp peak or broader maximum. We propose that in samples where the contact is wetted it grows continuously by pressure solution, forming the visible contact seen after the first 24 h of the experiment. This would explain the behaviour of samples a, b and d. In these experiments, the maximum and subsequent decrease in resistance may result from the effect on contact resistance of competition between increasing contact width w and decreasing normal stress σ_n, bringing about increasing Z through increasing average fluid thickness δ and/or diffusion coefficient D. This would be consistent with the fact that contact resistance does not increase linearly with w/r, as expected from Eq. 2 assuming δ and D are constant (Fig. 4b), but is almost independent of w/r. A possible explanation for sample c, which shows the large resistance peak (Fig. 4a), is that the grain boundary fluid is drastically thinned or entirely expelled during initial formation of the continuous (invisible) contact. The subsequent drop in resistance and simultaneous development of the continuously growing contact observed in Expt. c may be the result of some kind of marginal dissolution process [4,6,9,12] allowing re-wetting of the boundary followed by grain boundary diffusional pressure solution. This interpretation of the peak resistance in Expt. c is supported by the fact that the apparent Z-values calculated immediately following the peak do not lie on the same trend as our other Z versus σ_n data (Fig. 5b).

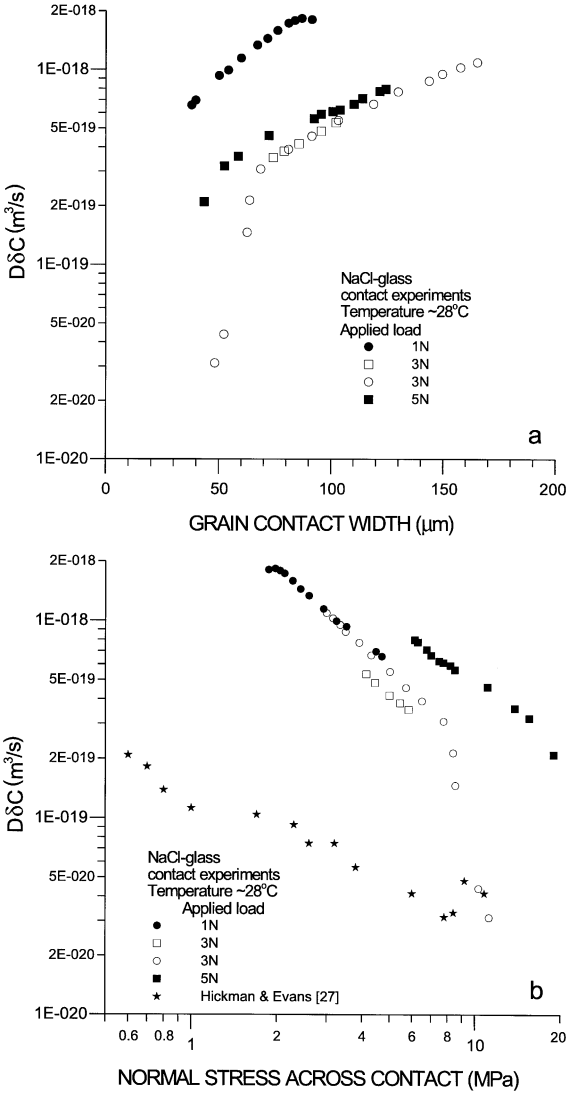

Fig. 5. (a) $D\delta C$ versus contact width (w); (b) $D\delta C$ versus normal stress across the contact (σ_n). Data plotted for the phase of continuous growth of the re-formed contact.

At present, it is unclear whether the near linear dependence of apparent Z-values on contact width and inverse dependence on normal stress (σ_n) in the post-peak phase of the experiments (Fig. 5a,b) is caused by changes of grain boundary fluid thickness (δ) and diffusivity with σ_n and/or time, a combined change of D, δ and C, and/or

a change of grain contact structure. It is evident from Fig. 5a,b, however, that initial load may also play a role in determining Z. This suggests a possible influence of initial contact stress or associated plastic deformation on subsequent grain boundary structure and properties.

As described in our optical observations, the machined conical surface of the hole in the NaCl crystals used shows idiomorphic overgrowth and concentric roughening which becomes more pronounced with time. The overgrowths are presumably at least partly due to the precipitation of NaCl removed from the contact by pressure solution. Local transport driven by the anisotropic surface energy of NaCl is believed to be responsible for the roughening, as the machined NaCl surface strives to minimize its surface energy through the formation of crystal ledges by short range diffusion (cf. [27]). As already indicated, we made no attempt to investigate the structure of the contact after the experiments, because there is no guarantee that the active contact structure is preserved during disassembly of the experiment. However, from the fact that no structures were optically visible within the contact during pressure solution, any internal roughness during pressure solution must have been less than 0.5–1 μm.

5.2. Comparison with previous work

The values for Z determined in the present study (3×10^{-20} m^3/s $< Z = D\delta C < 2\times10^{-18}$ m^3/s) by measuring the radial resistance of an actively pressure dissolving halite–glass contact, are in reasonable agreement with (though somewhat higher than) values for Z inferred from granular halite compaction experiments and previous experiments on halite–halite and halite–glass contacts at similar contact stresses and temperatures.

From wet halite compaction experiments, which showed good agreement with theoretical models for diffusion controlled pressure solution, Spiers and co-workers [9,21,33] obtained Z-values in the range 3×10^{-20}–3×10^{-19} m^3/s at room temperature, for grain contact stresses of 1–20 MPa. Inferring diffusion controlled pressure solution involving a thin grain boundary fluid film maintained by surface forces (disjoining pressure) in their halite–quartz glass contact experiments at 50°C, Hickman and Evans [27] calculated values for Z in the range 4×10^{-20}–2×10^{-19} m^3/s, for contact stresses of 0.5–12 MPa. Moreover, the inverse dependence of Z on σ_n observed in the present experiments was also observed by Hickman and Evans [27] (see Fig. 5b), who attributed this to the effect of σ_n on equilibrium film thickness as determined by surface forces. Shifting the 50°C Z-values obtained by Hickman and Evans [27] to the temperature of the experiments reported here, using the activation energy for Z of $\Delta H = 24.5$ kJ/mol obtained from experiments on polycrystalline NaCl aggregates by Spiers et al. [21], lowers the Hickman and Evans Z-values by half an order of magnitude. On the basis of halite–halite contact experiments at room temperature and with contact stresses of 1–7.5 MPa, Schutjens and Spiers [40] obtained Z-values in the range 5×10^{-20}–5×10^{-19} m^3/s for dissolving contacts showing little or no optical structure.

Our present Z-values therefore overlap with much of the previous data for Z, but are on average about one order of magnitude higher. We suggest that this discrepancy may be due to crystallographically controlled, periodic variations in grain boundary roughness, mean fluid thickness and/or fluid film structure/diffusivity around the circular contact, yielding a (high) composite value of Z. We have no direct evidence for this but consider it likely since the contact surface cuts all crystallographic directions at an angle of 45° to [001], producing a periodic variation in contact orientation. The effect of initial load on the Z versus σ_n data seen in our experiments may indicate that in our tests surface roughness, related to initial contact stress and plastic strain, played a role. As in previous work, the experiments reported here do not enable us to resolve the structure of the grain contact during pressure solution, or to separate values of D, δ, and C. However, we are presently performing Fourier transform infrared (FTIR) microanalysis experiments to determine independently the thickness of grain boundary fluid within actively pressure-dissolving halite–glass contacts. We are also extending our resistivity technique to determine $Z = D\delta C$ for

quartz–quartz contacts undergoing pressure solution in a hydrothermal cell.

A noteworthy implication of the inverse linear dependence of $Z = D\delta C$ on normal stress (σ_n) seen in the experiments reported here and in those of Hickman and Evans [27], is that the pressure solution creep rate is predicted to become independent of stress, when this dependence is inserted into a classical rate model for pressure solution creep [4,7,33,41]. This is not the case in polycrystalline NaCl which shows a near linear strain rate versus stress relation during creep by pressure solution [9,21,22,33]. However, in the experiments reported here and by Hickman and Evans [27], the contacts are NaCl–glass contacts, whereas in experiments on polycrystalline aggregates, grain boundaries are formed by NaCl–NaCl contacts. This suggests that the observed inverse dependence of $Z = D\delta C$ on σ_n may be a property of wetted halite–glass contacts only, reflecting the interaction of surface forces such as electrical double layer forces, hydration forces and Van der Waals forces [27]. Using FTIR microanalysis, we are expecting to be able to determine the fluid content and structure of both NaCl–glass and NaCl–NaCl contacts independently.

6. Conclusions

In the experiments presented here, loading the annular halite–glass contact probably led to plastic deformation and subsequent dissolution of contact points, sooner or later followed by growth of a continuous contact by steady grain boundary diffusional pressure solution. We have succeeded in measuring the electrical resistance of these continuous contacts during the active pressure solution stage of the tests. From these measurements and by making use of the Nernst–Einstein equation we have been able to calculate the magnitude of $Z = D\delta C$ after continuous contact formation, obtaining values in the range 3×10^{-20} m^3/s $< D\delta C < 2\times10^{-18}$ m^3/s. These values overlap with, though are typically one order of magnitude higher than, values reported in the literature for halite–halite and halite–glass contact experiments and obtained in granular halite compaction experiments. We have also found an inverse stress dependence of Z similar to that reported by Hickman and Evans [27]. The tests reported here do not enable us to elaborate on the internal structure of the actively dissolving contact or to evaluate D, δ, and C independently. ***[RV]***

References

[1] M.S. Paterson, Thermodynamics and its geological applications, Rev. Geophys. 11 (1973) 355–389.
[2] M.S. Paterson, A theory for granular flow accommodated by material transfer via an intergranular fluid, Tectonophysics 245 (1995) 135–152.
[3] E.H. Rutter, The kinetics of rock deformation by pressure solution, Philos. Trans. R. Soc. London A 283 (1976) 203–219.
[4] E.H. Rutter, Pressure solution in nature, theory and experiment, J. Geol. Soc. London 140 (1983) 725–740.
[5] P.Y. F Robin, Pressure-solution at grain-to-grain contacts, Geochim. Cosmochim. Acta 42 (1978) 1381–1389.
[6] H.W. Green, Pressure solution creep: some causes and mechanisms, J. Geophys. Res. 89 (1984) 4313–4318.
[7] F.K. Lehner, Thermodynamics of rock deformation by pressure solution, in: D. Barber, P. Meredith (Eds.), Deformation Processes in Minerals, Ceramics and Rocks, Unwin Hyman, London, 1990, pp. 296–333.
[8] F.K. Lehner, A model for intergranular pressure solution in open systems, Tectonophysics 245 (1995) 153–170.
[9] C.J. Spiers, R.H. Brzesowsky, Densification behaviour of wet granular salt: theory versus experiment, in: Seventh Symp. On Salt, Vol. I, 1993, pp. 83–92.
[10] S. de Meer, C.J. Spiers, Creep of wet gypsum aggregates under hydrostatic loading conditions, Tectonophysics 245 (1995) 171–184.
[11] S. de Meer, C.J. Spiers, Influence of pore-fluid salinity on pressure solution creep in gypsum, Tectonophysics 308 (1999) 311–330.
[12] R. Tada, R. Maliva, R. Siever, A new mechanism for pressure solution in porous quartzose sandstone, Geochim. Cosmochim. Acta 51 (1987) 2295–2301.
[13] N.H. Sleep, M.L. Blanpied, Creep, compaction and the weak rheology of major faults, Nature 359 (1992) 687–692.
[14] S.H. Hickman, B. Evans, Growth of grain contacts in halite by solution transfer: implication for diagenesis, lithification, and strength recovery, in: B. Evans, T.-W. Wong (Eds.), Fault Mechanics and Transport Properties of Rocks, Academic Press, San Diego, CA, 1992, pp. 253–280.
[15] S.H. Hickman, R. Sibson, R. Bruhn, Introduction to special section: mechanical involvement of fluids in faulting, J. Geophys. Res. 100 (1995) 12831–12840.
[16] S.L. Karner, C. Marone, B. Evans, Laboratory study of

fault healing and lithification in simulated fault gouge under hydrothermal conditions, Tectonophysics 277 (1997) 41–55.
[17] B. Bos, C.J. Spiers, Effect of clays on fluid-assisted healing behaviour of gouge-bearing faults, Earth Planet. Sci. Lett. 184 (2000) 199–210.
[18] B. Bos, C.J. Peach, C.J. Spiers, Slip behavior of simulated gouge-bearing faults under conditions favoring pressure solution, J. Geophys. Res. 105 (2000) 16699–16717.
[19] D. Elliot, Diffusion flow laws in metamorphic rocks, Bull. Geol. Soc. Am. 84 (1973) 2645–2664.
[20] B. Stöckhert, M. Wachmann, M. Küster, S. Bimmerman, Low effective viscosity during high pressure metamorphism due to dissolution precipitation creep; the record of HP-LT metamorphic carbonates and siliciclastic rocks from Crete, Tectonophysics 303 (1999) 299–319.
[21] C.J. Spiers, P.M.T.M. Schutjens, R.H. Brzesowsky, C.J. Peach, J.L. Liezenberg, H.J. Zwart, Experimental determination of constitutive parameters governing creep of rocksalt by pressure solution, in: R.J. Knipe, E.H. Rutter (Eds.), Deformation Mechanisms, Rheology and Tectonics, Geol. Soc. London Spec. Publ. 54 (1990) 215–227.
[22] C.J. Spiers, N.L. Carter, Microphysics of rocksalt flow in nature, in: M. Aubertin, H.R. Hardy (Eds.), The Mechanical Behaviour of Salt: Proceedings of the Fourth Conference. Series on Rock and Soil Mechanics, Vol. 22, TTP Trans Tech Publications, Clausthal-Zellerfeld, 1998, pp. 115–128.
[23] R. Raj, Creep in polycrystalline aggregates by matter transport through a liquid phase, J. Geophys. Res. 87 (1982) 4731–4739.
[24] S. de Meer, C.J. Spiers, Uniaxial compaction creep of wet gypsum aggregates, J. Geophys. Res. 102 (1997) 875–891.
[25] P.K. Weyl, Pressure solution and force of crystallization – a phenomenological theory, J. Geophys. Res. 64 (1959) 2001–2025.
[26] S.H. Hickman, B. Evans, Experimental pressure solution in halite: the effect of grain/interphase structure, J. Geol. Soc. London 148 (1991) 549–560.
[27] S.H. Hickman, B. Evans, Kinetics of pressure solution at halite-silica interfaces and intergranular clay films, J. Geophys. Res. 100 (1995) 13113–13132.
[28] F. Renard, P. Ortoleva, Water films at grain-grain contacts; Debye-Hückel osmotic model of stress, salinity, and mineralogy dependence, Geochim. Cosmochim. Acta 61 (1997) 1963–1970.
[29] V.Y. Traskin, Z.N. Skvortsova, Model concepts and experimental data on the transport of liquids along the boundaries of polycrystal grains, Colloid J. 59 (1997) 767–772.
[30] A.J. Gratz, Solution transfer compaction of quartzites: progress towards a rate law, Geology 19 (1991) 901–904.
[31] S.J.W. den Brok, An experimental investigation into the effect of water on the flow of quartzite, Ph.D. thesis, Geologica Ultraiectina 85 (1992) 178 pp.
[32] R. Raj, C.K. Chyung, Solution-precipitation creep in glass ceramics, Acta Metall. 29 (1981) 159–166.
[33] C.J. Spiers, P.M.T.M. Schutjens, Densification of crystalline aggregates by fluid phase diffusional creep, in: D. Barber, P. Meredith (Eds.), Deformation Processes in Minerals, Ceramics and Rocks, Unwin Hyman, London, 1990, pp. 334–353.
[34] Z.M. Jin, H.W. Green, Y. Zhou, Melt topology in partially molten mantle peridotite during ductile deformation, Nature 372 (1994) 164–167.
[35] P.M.T.M. Schutjens, Experimental compaction of quartz sand at low effective stress and temperature conditions, J. Geol. Soc. London 148 (1991) 527–539.
[36] A.M. Mullis, Determination of the rate-limiting mechanism for quartz pressure solution, Geochim. Cosmochim. Acta 57 (1993) 1499–1503.
[37] T. Dewers, A. Hajash, Rate laws for water-assisted compaction and stress-induced water-rock interaction in sandstones, J. Geophys. Res. 100 (1995) 13093–13112.
[38] F. Renard, P. Ortoleva, J.P. Gratier, Pressure solution in sandstones: influence of clays and dependence on temperature and stress, Tectonophysics 280 (1997) 257–266.
[39] J.O'M. Bockris, A.K.N. Reddy, Modern Electrochemistry, Vol. 1, Plenum, New York, 1977, 622 pp.
[40] P.M.T.M. Schutjens, C.J. Spiers, Intergranular pressure solution in NaCl: grain-to-grain contact experiments under the optical microscope, Oil Gas Sci. Tech. Rev. IFP 54 (1999) 729–750.
[41] S. de Meer, C.J. Spiers, Mechanisms and kinetics of creep by intergranular pressure solution, in: B. Jamtveit, P. Meakin (Eds.), Growth, Dissolution and Pattern Formation in Geosystems, Kluwer Academic Publishers, Dordrecht, 1999, pp. 345–363.